STUDY OF VIBRATIONAL DYNAMICS OF Ca-BASED METALLIC GLASSES BY PSEUDOPOTENTIAL THEORY

ADITYA M. VORA

Parmeshwari 165, Vijaynagar Area, Hospital Road,
Bhuj – Kutch, 370 001, Gujarat, INDIA
e-mail: voraam@yahoo.com

Received February 2, 2007

The vibrational dynamics of three Ca-based metallic glasses viz. $Ca_{70}Mg_{30}$, $Ca_{70}Zn_{30}$ and $Ca_{60}Al_{40}$ have been studied at room temperature in terms of the phonon eigen frequencies of longitudinal and transverse modes, employing three theoretical formulations given by Hubbard-Beeby (HB), Takeno-Goda (TG) and Bhatia-Singh (BS). Five local field correction functions viz. Hartree (H), Taylor (T), Ichimaru-Utsumi (IU), Farid *et al.* (F) and Sarkar *et al.* (S) are used for the first time in the present investigation to study the screening influence on the aforesaid properties. Long wavelength limits of the phonon modes are then used to get information on the elastic and thermal properties of the system. The low temperature specific heat is also calculated from the elastic limit of the phonon dispersion curves. The present results agree satisfactory with the experimental as well as theoretical values.

Key words: effective pair potential, phonon dispersion curves, pseudopotential, elastic and thermodynamic properties, metallic glasses.

INTRODUCTION

During the several decades, considerable theoretical development taken place in the field of disordered condensed matter physics. Generally, in this field the disorder means it is a periodic random structure. The few examples of this system are crystals with impurities, liquid metals, binary alloys, metallic glasses etc. The disordered materials are also known as non-crystalline materials. Moreover, the metallic glasses play an important role in the field of materials science and engineering, which opens the door of research for both theoretical and experimental persons. Such solids have electronic properties normally associated with metals but atomic arrangement is not periodic. They made up of two components of metals provide us physically interesting system for theoretical investigations. Based on the knowledge of interatomic interactions we can understand the thermodynamic, mechanical and electronic transport properties of amorphous solids. Such investigations involve measurements of collective density waves at larger momenta and for a few metallic glasses it is

possible to measure the dynamical structure factors upto very large wave vectors [1–13]. Recently, Vora *et al.* [1–3] have been studied the vibrational properties of some binary metallic glasses.

Keeping all this in mind, the theoretical investigations on the vibrational dynamics of three Ca-based amorphous binary metallic glasses viz. $Ca_{70}Mg_{30}$, $Ca_{70}Zn_{30}$ and $Ca_{60}Al_{40}$ have been reported in the present paper. There are three main theoretical approaches used to compute the phonon frequencies of alloys: one is the phenomenological theory of Hubbard-Beeby (HB) [14] in the random phase approximation, second approach is the quasi crystalline approximation technique with interatomic pair potential developed by Takeno-Goda (TG) [15] and third is by evaluation of force constants as was done by Bhatia-Singh (BS) [16, 17].

In the present investigation, the well recognized empty core model (EMC) potential of Ashcroft [18] used to explain the electron-ion interaction in the study of metallic glasses is given by [18],

$$W(q) = \frac{-4\pi Ze^2}{\Omega_o q^2 \varepsilon(q)} \cos\left(qr_C\right). \tag{1}$$

Where r_C is the parameter of the potential, Z the valence and $\varepsilon(q)$ the modified Hartree dielectric function. The model potential parameter r_C is calculated from the well known formula [1–3] as follows:

$$r_C = \left[\frac{0.51\, r_S}{(Z)^{1/3}}\right]. \tag{2}$$

Here r_S is the effective Wigner-Seitz radius of the component, respectively.

Five local field correction functions viz. Hartree (H) [19], Taylor (T) [20], Ichimaru-Utsumi (IU) [21], Farid *et al.* (F) [22] and Sarkar *et al.* (S) [23] are used for the first time in the present investigation to study the screening influence on the aforesaid properties. Besides, the thermodynamic properties such as longitudinal sound velocity (υ_L), transverse sound velocity (υ_T) and Debye temperature (θ_D), low temperature specific heat capacity (C_V) and some elastic properties viz. the isothermal bulk modulus (B_T), modulus of rigidity (G), Poisson's ratio (σ) and Young's modulus (Y) are also calculated from the elastic part of the phonon dispersion curves (PDC). Finally a comparison is made between the computed results and available theoretical as well as experimental data.

$Ca_{70}Mg_{30}$ is the most important candidate of simple metallic glasses. The phonon dispersion curves (PDC) of this glass has been investigated by many workers theoretically using the pseudopotential theory [1, 2, 6–11] as well as experimentally [5]. The $Ca_{70}Mg_{30}$ glass has been theoretically investigated by

Hafner [14] and Hafner-Jaswal [15] on the basis of $S(\mathbf{q}, \omega)$ and by BS approach using a model approach and assuming the force among nearest neighbours as central and volume dependent. Saxena *et al.* [8, 9] have studied the PDC of this glass using the HB and TG approaches with effective pair potential (EPP) and effective atom model (EAM) models. In these entire calculations Ashcroft's empty core model potential [18] is used. Also Agarwal *et al.* [10, 11] have calculated the PDC of the glass using BS approach. Thakore *et al.* [4] have also been studied the PDC and their related properties of the glass using HB approach with EAM model. Recently, Vora *et al.*[1, 2] have been studied the vibrational properties of $Ca_{70}Mg_{30}$ binary metallic glass. In all these calculations, they have noted that, their results are in a very good agreement with the reported experimental or theoretical findings. Similarly from the literature survey, It can be noted that, nobody have reported the experimental as well as theoretical work related to PDC of $Ca_{70}Zn_{30}$ and $Ca_{60}Al_{40}$ glasses in our knowledge. The structural and electronic properties of $Ca_{70}Zn_{30}$ glass have been studied by Tegze and Hafner [12]. They have adopted ab initio pseudopotential as well as MD techniques to study the electronic structure of the glass. The atomic and electronic structure of $Ca_{60}Al_{40}$ glass is studied by Hafner and Jaswal [13]. These calculations are based on realistic models for the atomic structure constructed by MD simulation.

METHOD OF COMPUTATION

The fundamental ingredient, which goes into the calculation of the phonon dynamics of simple metallic glasses, is the effective pair potential, which consists of two contributions. One is the direct interaction between ions given by $\left(Z e^2/r\right)$ while the other contribution is due to the indirect interaction between ions through the electron cloud. The indirect interaction is calculated using the normalized energy wave number characteristics.

The effective interatomic pair potential for the amorphous binary alloys can be found the binary system as a one component metallic fluid, *i.e.* the concept of effective atom [1–4]. In this concept a simple binary disordered system $A_X B_{1-X}$ can be looked upon as an assembly of the effective atom (*i.e.* one component system). In the present study we have considered here all the glasses as a one component fluid for investigating the phonon frequencies and their related elastic and thermodynamic properties.

The effective interaction in the glass can be written as [1–4],

$$V_{eff}(r) = \left(\frac{Z_{eff}^2 e^2}{r}\right) + \frac{\Omega_{oeff}}{\pi^2} \int F_{eff}(q) \left[\frac{Sin(qr)}{qr}\right] q^2 dq. \tag{3}$$

Here Z_{eff} and Ω_{oeff} are the effective valence and atomic volume of the one component fluid respectively, given by [1–4]

$$Z_{eff} = X Z_A + (1-X) Z_B , \tag{4}$$

and

$$\Omega_{oeff} = X \Omega_{oA} + (1-X) \Omega_{oB} . \tag{5}$$

Where X is the concentration of first component of the glass.

The energy wave number characteristics appearing in the equation (3) is written as [1–4]

$$F_{eff}(q) = \frac{-\Omega_{oeff} q^2}{16\pi} \left| W_B^{eff}(q) \right|^2 \frac{\left[\varepsilon_H^{eff}(q) - 1 \right]}{\left\{ 1 + \left[\varepsilon_H^{eff}(q) - 1 \right] \left[1 - f_{eff}(q) \right] \right\}} . \tag{6}$$

Here $W_B^{eff}(q)$ is the effective bare ion potential, $\varepsilon_H^{eff}(q)$ the Hartree dielectric response function and $f_{eff}(q)$ the local field correction function to introduce the exchange and correlation effects. A quantity which is equally important as the pair potential while studying a disorder system is the pair correlation function $g(r)$, which is computed theoretically from the effective pair potentials [1–4].

The recent investigations to study the vibrational dynamics of amorphous system have shown that any first-principle theory to study the propagation of phonons in amorphous solids is much more accurate and close to the experimental investigations than those based on parametric calculations. In a view of this, the three theories of phonons in amorphous solids as developed by Hubbard-Beeby (HB) [14], Takeno-Goda (TG) [15] and Bhatia-Singh (BS) [16, 17] have been employed for studying the longitudinal and transverse phonon frequencies in the present study.

According to the HB, the expressions for longitudinal $(\omega_L(q))$ and transverse $(\omega_T(q))$ phonon frequencies are [1–4, 14],

$$\omega_L^2(q) = \omega_E^2 \left[1 - \frac{\sin(q\sigma)}{q\sigma} - \frac{6\cos(q\sigma)}{(q\sigma)^2} + \frac{6\sin(q\sigma)}{(q\sigma)^3} \right], \tag{7}$$

$$\omega_T^2(q) = \omega_E^2 \left[1 - \frac{3\cos(q\sigma)}{(q\sigma)^2} + \frac{3\sin(q\sigma)}{(q\sigma)^3} \right]. \tag{8}$$

with $\omega_E^2 = \left(\frac{4\pi\rho_{eff}}{3M_{eff}} \right) \int_0^\infty g(r) V_{eff}''(r) r^2 dr$ is the maximum frequency.

The expressions for longitudinal $(\omega_L(q))$ phonon frequency and transverse $(\omega_T(q))$ phonon frequency as per TG approach are [1–3, 15],

$$\omega_L^2(q)=\left(\frac{4\pi\rho_{eff}}{M_{eff}}\right)\int_0^\infty dr\, g(r)\left[\left\{rV'_{eff}(r)\left(1-\frac{\sin(qr)}{qr}\right)\right\}+\left\{r^2V''_{eff}(r)-rV'_{eff}(r)\right\}\left(\frac{1}{3}-\frac{\sin(qr)}{qr}-\frac{2\cos(qr)}{(qr)^2}+\frac{2\sin(qr)}{(qr)^3}\right)\right], \tag{9}$$

$$\omega_T^2(q)=\left(\frac{4\pi\rho_{eff}}{M_{eff}}\right)\int_0^\infty dr\, g(r)\left[\left\{rV'_{eff}(r)\left(1-\frac{\sin(qr)}{qr}\right)\right\}+\left\{r^2V''_{eff}(r)-rV'_{eff}(r)\right\}\left(\frac{1}{3}+\frac{2\cos(qr)}{(qr)^2}+\frac{2\sin(qr)}{(qr)^3}\right)\right] \tag{10}$$

Recently BS approach was modified by Shukla and Campnaha [17]. They were introduced screening effects in the BS approach. Then, with the above assumptions and modification, the dispersion equations for an amorphous material can be written as [1–3, 16, 17]

$$\rho_{eff}\,\omega_L^2(q)=\frac{2N_{Ceff}}{q^2}(\beta I_0+\delta I_2)+\frac{k_e\,k_{TF}^2\,q^2\,\varepsilon(q)\left|G(qr_S)\right|^2}{q^2+k_{TF}^2\,\varepsilon(q)}, \tag{11}$$

and

$$\rho_{eff}\,\omega_T^2(q)=\frac{2N_{Ceff}}{q^2}\left(\beta I_0+\frac{1}{2}\delta(I_0-I_2)\right). \tag{12}$$

The other details of used constants in the BS approach were already narrated in the literature [16, 17]. Here M_{eff} is the effective atomic mass, ρ_{eff} the effective number density and N_{Ceff} the effective coordination number of the glassy system, respectively.

In the long-wavelength limit of the frequency spectrum, the both the frequencies *i.e.* transverse and longitudinal are proportional to the wave vectors and obey the relationships [1–4],

$$\begin{aligned}&\omega_L\propto q \quad\text{and}\quad \omega_T\propto q,\\ &\therefore\ \omega_L=\upsilon_L\,q \quad\text{and}\quad \omega_T=\upsilon_T\,q.\end{aligned} \tag{13}$$

Where υ_L and υ_T are the longitudinal and transverse sound velocities, in the glass respectively. For the three approaches the equations are:

For HB approach the formulations for υ_L and υ_T are given by [14],

$$\upsilon_L(HB) = \omega_E \sqrt{\frac{3\sigma^2}{10}}, \tag{14}$$

and

$$\upsilon_T(HB) = \omega_E \sqrt{\frac{\sigma^2}{10}}. \tag{15}$$

In TG approach the expressions for υ_L and υ_T are written by [15],

$$\upsilon_L(TG) = \left[\left(\frac{4\pi\rho_{eff}}{30\,M_{eff}}\right)\int_0^\infty dr\, g(r)\, r^3 \left\{ r V''(r) - 4V'(r)\right\}\right]^{1/2}, \tag{16}$$

and

$$\upsilon_T(TG) = \left[\left(\frac{4\pi\rho_{eff}}{30\,M_{eff}}\right)\int_0^\infty dr\; g(r)\, r^3 \left\{ 3r V''(r) - 4V'(r)\right\}\right]^{1/2}. \tag{17}$$

The formulations for υ_L and υ_T in BS approach are as follows [16, 17],

$$\upsilon_L(BS) = \left[\frac{N_{Ceff}}{\rho_a}\left(\frac{1}{3}\beta + \frac{1}{5}\delta\right) + \frac{k_e}{3}\right]^{1/2}, \tag{18}$$

and

$$\upsilon_T(BS) = \left[\frac{N_{Ceff}}{\rho_a}\left(\frac{1}{3}\beta + \frac{1}{15}\delta\right)\right]^{1/2}. \tag{19}$$

In the long-wavelength limit of the frequency spectrum, transverse and longitudinal sound velocities υ_L and υ_T are computed. The isothermal bulk modulus B_T, modulus of rigidity G, Poisson's ratio σ, Young's modulus Y and the Debye temperature θ_D are found using the expressions [1–4],

$$B_T = \rho_M\left(\upsilon_L^2 - \frac{4}{3}\upsilon_T^2\right), \tag{20}$$

$$G = \rho_M\,\upsilon_T^2. \tag{21}$$

With ρ_M is the isotropic number density of the solid.

$$\sigma = 1 - 2\left(\frac{\upsilon_T^2}{\upsilon_L^2}\right)\Big/ 2 - 2\left(\frac{\upsilon_T^2}{\upsilon_L^2}\right), \tag{22}$$

$$Y = 2G(\sigma + 1), \tag{23}$$

$$\theta_D = \frac{\hbar\omega_D}{k_B} = \frac{\hbar}{k_B} 2\pi \left[\frac{9\rho_{eff}}{4\pi}\right]^{1/3} \left[\frac{1}{\upsilon_L^3} + \frac{2}{\upsilon_T^3}\right]^{(-1/3)}. \quad (24)$$

here ω_D is the Debye frequency.

The low temperature specific heat C_V can be calculated from the following expressions [1–3],

$$C_V = \frac{\Omega_{Oeff}\,\hbar^2}{k_B T^2} \sum_{\lambda=L,T} \int \frac{d^3q}{(2\pi)^3} \frac{\omega_\lambda^2(q)}{\left[\exp\left(\frac{\hbar\omega_\lambda(q)}{k_B T}\right)-1\right]\left[1-\exp\left(-\frac{\hbar\omega_\lambda(q)}{k_B T}\right)\right]}. \quad (25)$$

RESULTS AND DISCUSSION

The input parameters and other related constants used in the present computations are shown in Table 1. The effective interatomic pair potentials, the phonon dispersion curves (PDC) and graphical representations of the low temperature specific heat capacity (C_V) are displayed in Figs. 1–12 for each metallic glass.

Table 1

Input Parameters and constants

Glass	Z_{eff}	N_C	M_{eff} (amu)	Ω_0 (au)	ρ_M (gm/cm^3)	r_C (au)
$Ca_{70}Mg_{30}$	2.00	12.00	35.35	246.07	1.6091	1.2592
$Ca_{70}Zn_{30}$	2.00	12.00	47.67	221.86	2.4070	1.2317
$Ca_{60}Al_{40}$	2.40	12.00	34.84	218.52	1.7861	1.1073

The effective interatomic pair potential of the $Ca_{70}Mg_{30}$ glass is shown in Fig. 1. It is seen from the figure that, the effective interatomic pair potentials have significant oscillations in the larger *r*-region and also it shows fair agreement with the others [6, 8, 9]. The first zero for $V(r = r_0)$ due to H-function occurs at $r_0 = 8.4$au, while inclusion of exchange and correlation suppresses this zero and occurs that at $r_0 \leq 4.5$au. The well width and the position of $V_{min}(r)$ are also affected by the nature of the screening. The maximum depth in the pair potential is obtained for S-function and moved towards the left as compared to the potentials of Hafner [14] and Saxena *et al.* [16]. The results of Saxena *et al.* [16] show significant oscillations and potential energy remains positive in the large *r*-region. Thus Coulomb repulsive potential part dominates the oscillations due to ion-electron-ion interactions in their studies.

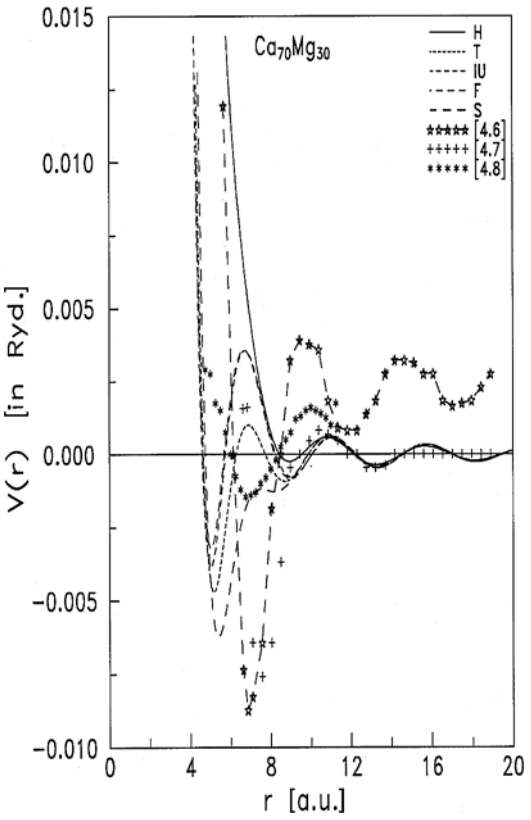

Fig. 1 – Pair Potentials for $Ca_{70}Mg_{30}$ Glass.

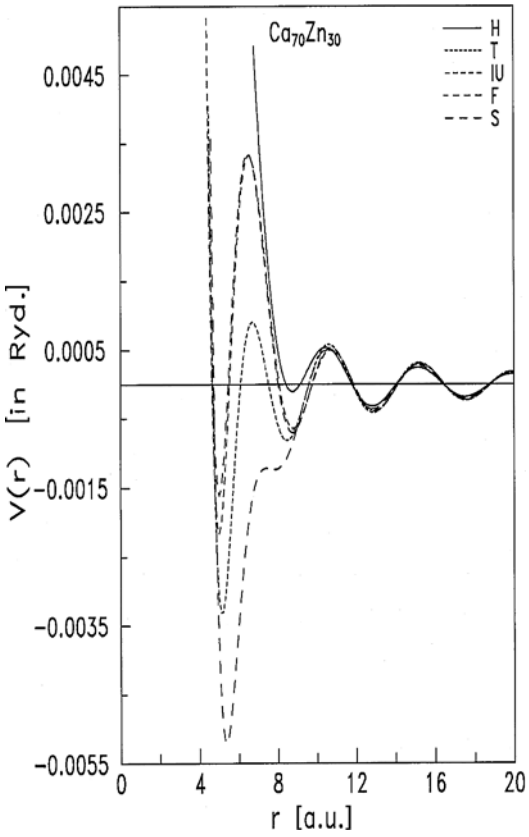

Fig. 2 – Pair Potentials for $Ca_{70}Zn_{30}$ Glass.

The presently computed pair potentials of $Ca_{70}Zn_{30}$ glass are shown in Fig. 2. The first zero for $V(r = r_0)$ due to H occurs at $r_0 = 8.4$au, while inclusion of exchange and correlation suppresses this zero and occurs that at $r_0 \leq 4.6$au. The inclusion of exchange and correlation effects increases the well width of $V(r)$ compared to H-screening function and also affects the position of $V_{min}(r)$. The maximum depth in the pair potential is obtained for S-function, while minimum is for H-screening function. The pair potential curves of $Ca_{70}Zn_{30}$ show hardcore nature.

The presently computed pair potentials of $Ca_{60}Al_{40}$ glass are shown in Fig. 3 alongwith the other such results [13]. In the present study the maximum depth in the pair potential is obtained for S-function. The first zero for $V(r = r_0)$ due to H-function occurs at $r_0 = 7.7$au, while the inclusion of exchange and correlation function suppresses this to $r_0 \leq 4.6$au. The position of $V_{min}(r)$ is also affected by the nature of the screening. It is observed that the position of first

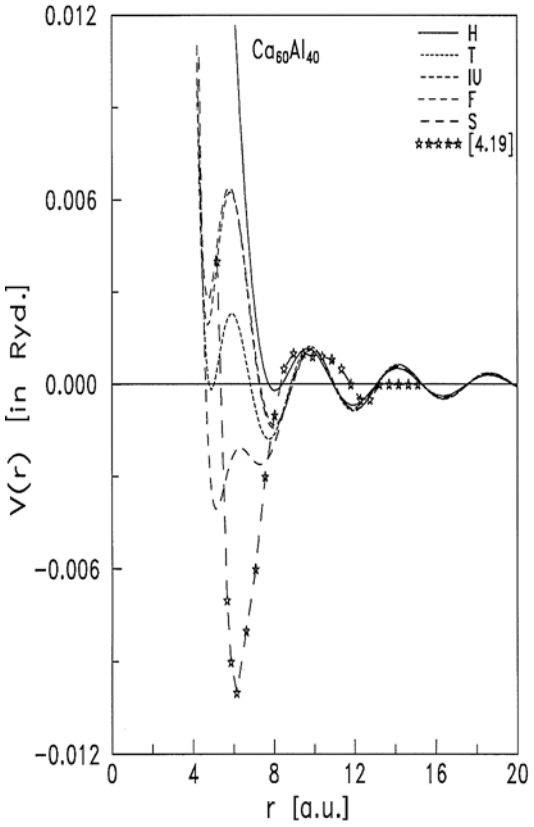

Fig. 3 – Pair Potentials for $Ca_{60}Al_{40}$ Glass.

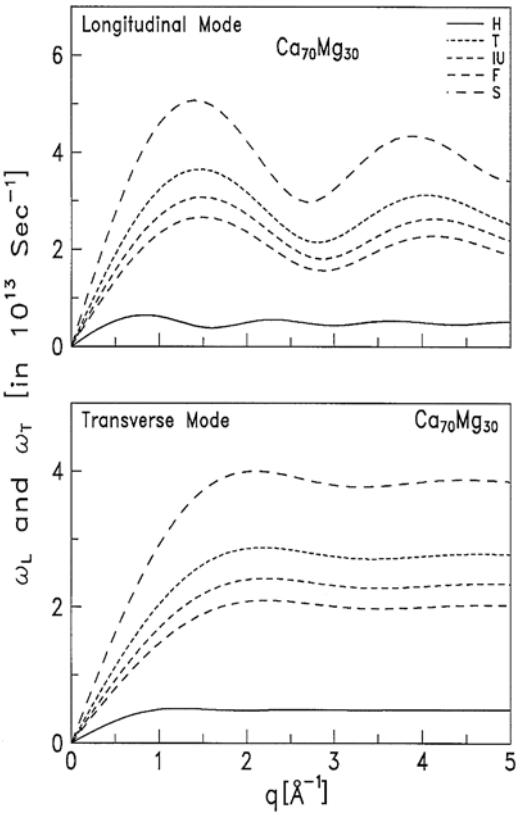

Fig. 4 – Screening influence on phonon dispersion curves of $Ca_{70}Mg_{30}$ Glass.

minimum of pair potentials in present computations moved towards the left in contrast to Hafner and Jaswal [22]. They have obtained very deep minimum in their study while present model potential generates shallow minimum in $V(r)$.

Also one important feature can be noted from the Figs. 1–3 that, when we moved from $Ca_{70}Mg_{30} \rightarrow Ca_{60}Al_{40}$ glass the as effective valence Z_{eff} increases the depth position shifts towards higher r-values. These show the strong dependency of depth position of effective interatomic pair potential on effective valence Z_{eff}.

The phonon eigen frequencies for longitudinal and transverse phonon modes calculated using HB approach with the five screening functions are shown in Fig. 4 to study the screening influences for $Ca_{70}Mg_{30}$ glass. It is seen from Fig. 4 that, the inclusion of exchange and correlation effects enhances the phonon frequencies in both longitudinal and transverse branches. The present results of PDC due to T, IU and F-functions are lying between those due to H

and S-screening. The first minimum in the longitudinal branch is around at $q \approx 1.6$ Å^{-1} for H, $q \approx 2.8$ Å^{-1} for T, $q \approx 2.9$ Å^{-1} IU and F and $q \approx 2.7$ Å^{-1} for S-local field correction function. The influence of various screening functions on ω_L at first peak on PDC with respect to H-screening is 464.65% for T, 375.94% for IU, 312.13% for F and 685.73% for S-screening. The same influence on ω_T at $q \approx 1.0$ Å^{-1} due to T-dielectric function is 309.70%, for IU is 239.86%, for F is 194.27% and for S-screening is 486.56%.

The PDC due to three approaches (HB, TG, BS) with S-local field correction function are shown in Fig. 5 for $Ca_{70}Mg_{30}$ glass. It is observed from the Fig. 5 that, the oscillations are more prominent in the longitudinal phonon modes as compared to the transverse modes in all three approaches. This shows the existence of collective excitations at larger momentum transfer due to longitudinal phonons only and the instability of the transverse phonons due to the anharmonicity of the atomic vibrations in the metallic systems. Moreover, the present outcome of both the phonon modes due to HB and TG approaches are more enhances than due to BS approach. The first plunge in the longitudinal branch falls at $q \approx 1.8$ Å^{-1} for BS, $q \approx 2.6$ Å^{-1} for TG and $q \approx 2.7$ Å^{-1} for HB approach. The first crossover position of ω_L and ω_T in the HB, TG and BS approaches are observed, respectively, at 2.1 Å^{-1}, 1.9 Å^{-1} and 1.2 Å^{-1}. The presently computed values are compared with experimental [5] and theoretical results of Hafner [6] and others [8–10]. It is apparent from the Fig. 5 that, the position of first peak obtained with the help of HB and TG approaches are closer to each other but their results are differing from each other substantially. It is also evident that the modes due to HB and BS approaches are suppressed in contrast to TG approach. Compared to the results reported by Hafner [14] which overestimates the experimental results, the present theoretical results of BS approach are found quite satisfactory with the experimental data of Suck *et al.* [5] and others [6, 8–10].

The results shown in Fig. 6 are the phonon frequencies of $Ca_{70}Zn_{30}$ glass generated using HB approach with the five screening functions for studying the screening influence. It is seen that the inclusion of exchange and correlation effect enhances the phonon frequencies in both longitudinal as well as transverse branches. The first minimum in the longitudinal branch is around at $q \approx 1.6$ Å^{-1} for H, $q \approx 2.8$ Å^{-1} for T, $q \approx 2.9$ Å^{-1} IU and F, $q \approx 2.8$ Å^{-1} for S-local field correction function. The variation of ω_L at first peak due to T-dielectric function is 306.17%, for IU is 231.87%, for F is 197.31% and for S-screening is 626.95% with respect to H-dielectric. The same variation on ω_T at $q \approx 1.0$Å^{-1} with respect to H-screening is 197.31% for T, 139.14% for IU, 114.19% for F and 357.14% for S-screening.

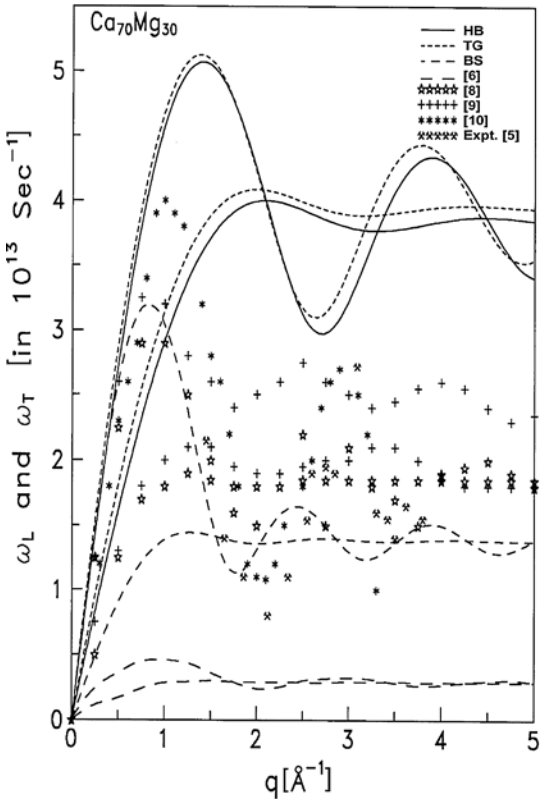

Fig. 5 – Phonon Dispersion Curves for $Ca_{70}Mg_{30}$ Glass.

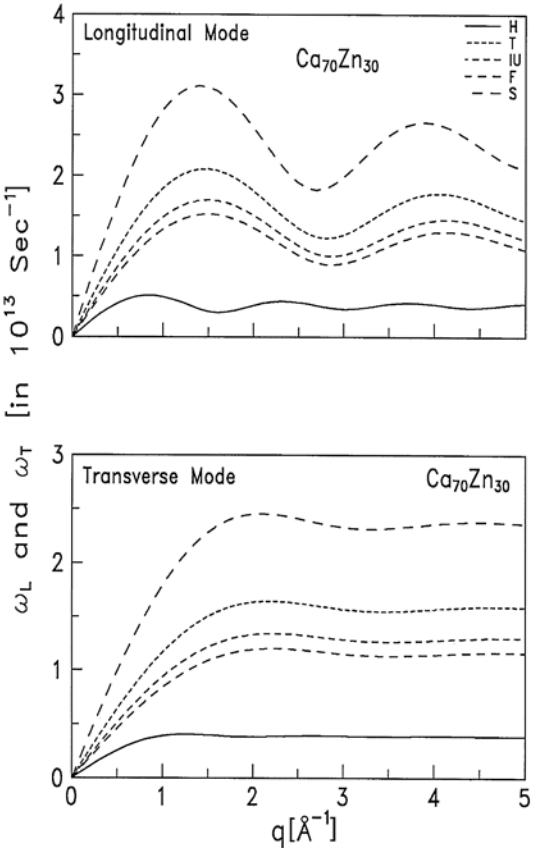

Fig. 6 – Screening influence on phonon dispersion curves of $Ca_{70}Zn_{30}$ Glass.

Fig. 7 is drawn to study the effect of three approaches (HB, TG and BS), where the results due to S-correction function is shown for $Ca_{70}Zn_{30}$ glass. It is observed that the oscillations are foremost in the longitudinal phonon modes as compared to the transverse mode in all three approaches. Moreover, the present outcome of ω_L and ω_T due to HB and TG approaches are enhanced than BS approach. The first immerse in the longitudinal branch falls at $q \approx 1.8$ Å^{-1} for BS, $q \approx 2.7$ Å^{-1} for TG and $q \approx 2.8$ Å^{-1} for HB approach. The first crossing point of ω_L and ω_T in the HB, TG and BS approaches are observed at 2.1 Å^{-1}, 2.1 Å^{-1} and 1.5 Å^{-1}, respectively.

To study the screening influence on the phonon eigen frequencies, the longitudinal and transverse phonon modes using HB approach for $Ca_{60}Al_{40}$ glass are shown in Fig. 8. The enhancement in both the phonon branches is concluded due to the effect of exchange and correlation functions. The present results of PDC

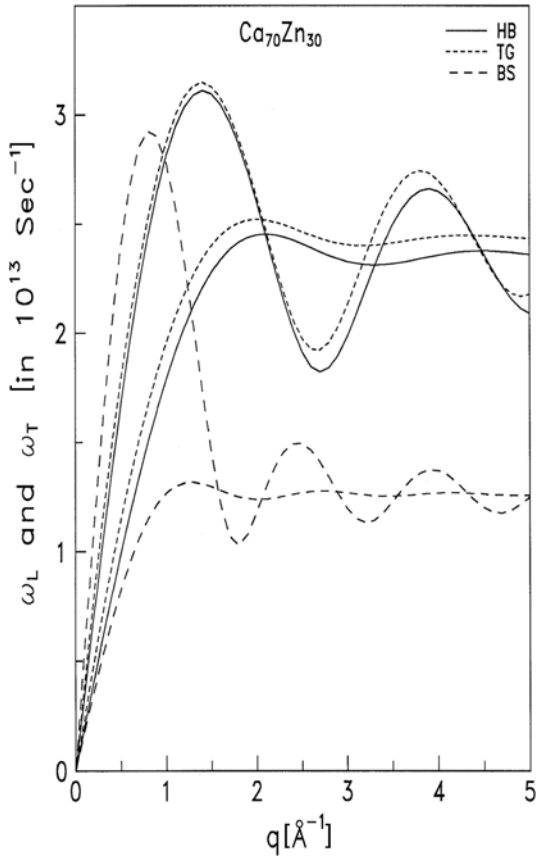

Fig. 7 – Phonon Dispersion Curves for $Ca_{70}Zn_{30}$ Glass.

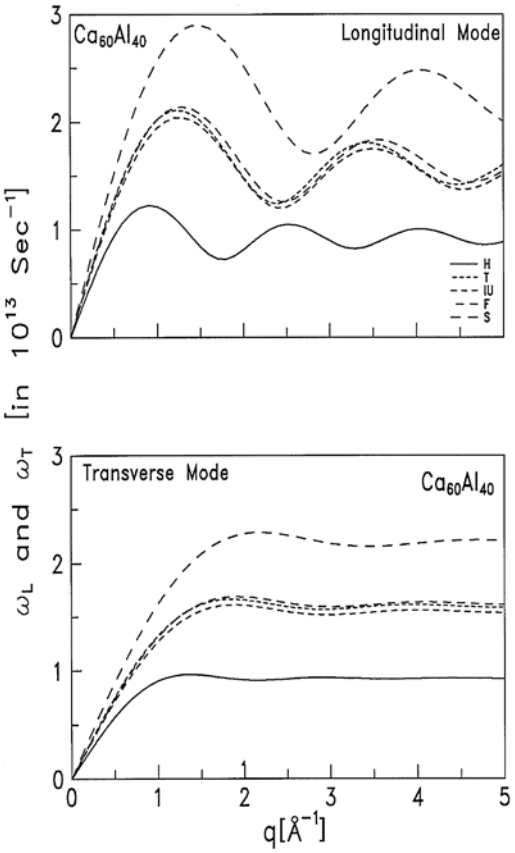

Fig. 8 – Screening influence on phonon dispersion curves of $Ca_{60}Al_{40}$ Glass.

due to T, IU and F-function are lying between those due to H and S-screening. The first minimum in the longitudinal branch is around at $q \approx 1.6$ Å^{-1} for H, $q \approx 2.4$ Å^{-1} for T and F, $q \approx 2.5$ Å^{-1} for IU and $q \approx 2.8$ Å^{-1} for S-local field correction function. At first peak, the screening influence on ω_L with respect to H-screening is 72.09% in the case of T-function, 66.41% in the case of IU-function, 71.55% in the case of F-function and 72.76% in the case of S-function. Such influence on ω_T at $q \approx 1.0$ Å^{-1} due to T-screening is 46.23%, for IU is 40.00%, for F is 44.98% and for S-screening is 78.64% with respect to H-dielectric function.

The PDC due to three approaches (HB, TG, BS) for $Ca_{60}Al_{40}$ glass are shown in Fig. 9. It is observed that the dispersion of the longitudinal phonons show oscillatory behaviour for large q-values while the transverse phonons show hardly any oscillatory behaviour to higher q-values *i.e.* transverse phonon behaviour

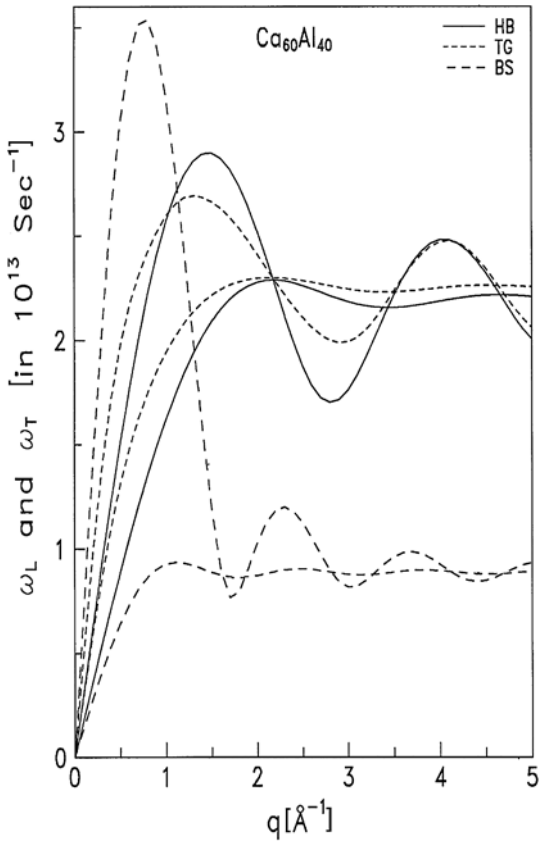

Fig. 9 – Phonon Dispersion Curves for $Ca_{60}Al_{40}$ Glass.

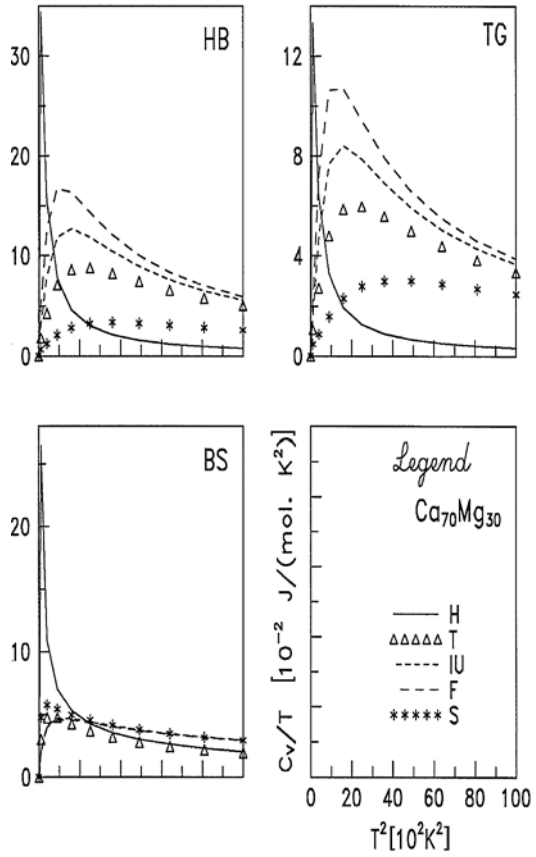

Fig. 10 – The Vibrational Part of the Specific Heat (C_V) of $Ca_{70}Mg_{30}$ Glass.

is monotonic at higher q. The first depth in the longitudinal branch occurs at $q \approx 1.6$ Å^{-1} for BS, $q \approx 2.9$ Å^{-1} for TG and $q \approx 2.8$ Å^{-1} for HB approach. The first crossover location of ω_L and ω_T in three approaches is observed at 2.2 Å^{-1}, 2.2 Å^{-1} and 1.6 Å^{-1}, respectively.

The PDC shows the existence of collective excitations at larger momentum transfer due to longitudinal phonons only and the instability of the transverse phonons due to the anharmonicity of the atomic vibrations in the metallic systems. Actually, Neutron Inelastic Scattering (NIS) experiments on $Mg_{70}Zn_{30}$ glass, by Suck *et al.* [5] have exposed vigorously low-lying short wavelength collective density excitation at wave vector transfer where the structure factor shows its main peak, which are called phonon-roton states [5]. The difference in the magnitude of the minimum around $2k_F$ seems to be due to the fact that the concept of roton has not been taken into account theoretically.

As shown in Fig. 10, the exchange and correlation functions also affect the anomalous behaviour (*i.e.* deviation from the T^3 law) which is observed in the vibrational part of the specific heat (C_V) for $Ca_{70}Mg_{30}$ glass. The reason behind the anomalous behaviour may be due to the low frequency modes modify the generalized vibrational density of states of the glass with that of the polycrystal. These modes are mainly responsible for the difference in the temperature dependence of the vibrational part of the specific heat which departs from the normal behaviour. For $Ca_{70}Zn_{30}$ glass, the $C_V/T \to T^2$ relation is shown in Fig. 11. For all the three approaches as temperature increases, the initial rise in specific heat is observed at low temperature region and then it decreases. This observation is deviated for S-screening in HB and TG approaches, where very high bump in C_V/T for low temperature is absent. The temperature dependence of $C_V(T)$ is drawn in Fig. 12 for $Ca_{60}Al_{40}$ glass. As temperature increases $C_V(T)$

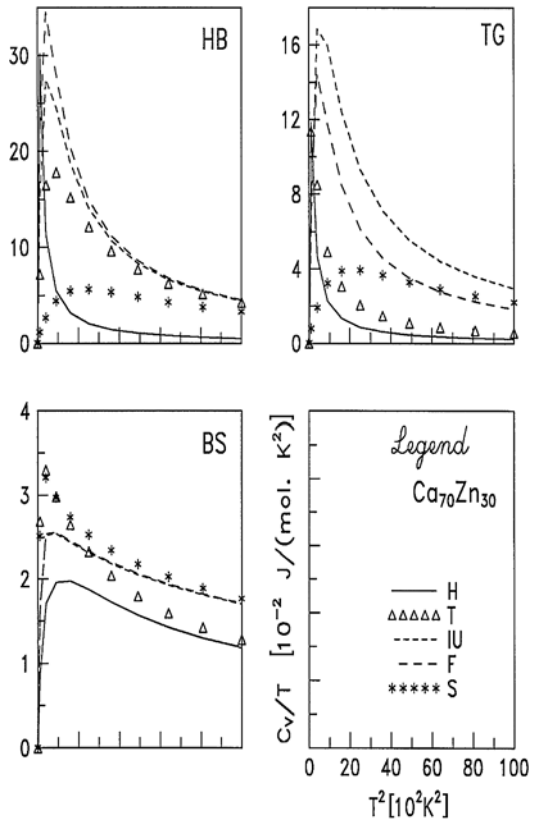

Fig. 11 – The Vibrational Part of the Specific Heat (C_V) of $Ca_{70}Zn_{30}$ Glass.

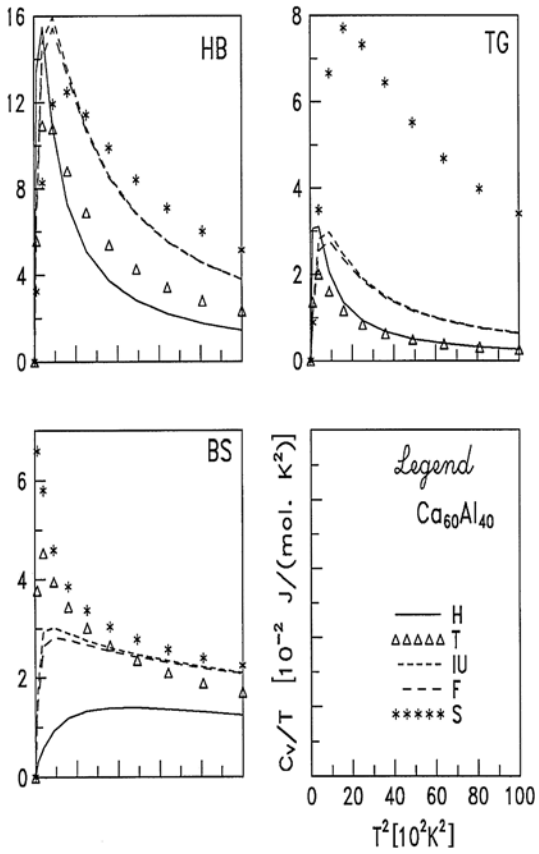

Fig. 12 – The Vibrational Part of the Specific Heat (C_V) of $Ca_{60}Al_{40}$ Glass.

for S-screening function shows high bump at low temperature region in the case of TG and BS approaches.

Furthermore, the thermodynamic and elastic properties estimated from the elastic part of the PDC are tabulated in Table 2. Among the five screening functions, the results of υ_L and υ_T are influenced more due to S-function. The comparison with other such results [5, 8] favours the present calculation and suggests that proper choice of dielectric screening is important part for explaining the thermodynamic and elastic properties of $Ca_{70}Mg_{30}$ glass.

Table 2

Thermodynamic and Elastic properties of $Ca_{70}Mg_{30}$ Metallic Glass

App.	SCR	$\upsilon_L \times 10^5$ cm/sec	$\upsilon_T \times 10^5$ cm/s	$B_T \times 10^{11}$ dyne/cm^2	$G \times 10^{11}$ dyne/cm^2	σ	$Y \times 10^{11}$ dyne/cm^2	θ_D (K)
HB	H	1.2474	0.7202	0.1391	0.0835	0.2499	0.2087	71.82
	T	3.9991	2.3089	1.4297	0.8578	0.2499	2.1445	230.25
	IU	3.3013	1.9060	0.9743	0.5846	0.2500	1.4615	190.07
	F	2.8585	1.6503	0.7305	0.4383	0.2500	1.0957	164.58
	S	5.7833	3.3390	2.9900	1.7940	0.2499	4.4850	332.97
TG	H	1.9214	1.1150	0.3273	0.2001	0.2461	0.4986	111.14
	T	4.8782	2.8780	2.0521	1.3329	0.2330	3.2869	286.44
	IU	4.2824	2.5199	1.5886	1.0218	0.2352	2.5241	250.86
	F	3.9697	2.3284	1.3726	0.8724	0.2378	2.1597	231.87
	S	6.3999	3.8498	3.4110	2.3850	0.2165	5.8025	382.46
BS	H	5.4736	2.3214	3.6649	0.8671	0.3903	2.4112	235.73
	T	5.2153	1.7023	3.7550	0.4663	0.4404	1.3433	174.03
	IU	5.4166	2.0037	3.8598	0.6461	0.4207	1.8358	204.32
	F	5.3318	1.9919	3.7231	0.6385	0.4189	1.8118	203.07
	S	5.1779	1.6787	3.7097	0.4534	0.4413	1.3071	171.64
Others [5, 8]		5.66, 4.67	3.55, 2.34	1.80 2.49	1.49 0.94	0.17 0.33	3.50 2.51	–

It is noticed from Table 3 for $Ca_{70}Zn_{30}$ glass that the υ_L and υ_T for HB and TG approaches are influenced significantly by various exchange and correlation functions as compare for BS approach. However, very high compressibility is observed for BS approach. As υ_L and υ_T are depend on the nature of screening as well as the method adopted, the other thermodynamic and elastic properties are also reflecting the same behaviour.

From the elastic limit of the PDC, the thermodynamic and elastic properties for $Ca_{60}Al_{40}$ glass are calculated and shown in Table 4. The compressibility B_T affects largely by S-screening in HB approach as compare to others.

Table 3

Thermodynamic and Elastic properties of $Ca_{70}Zn_{30}$ Metallic Glass

App.	SCR	$\upsilon_L \times 10^5$ cm/sec	$\upsilon_T \times 10^5$ cm/s	$B_T \times 10^{11}$ dyne/cm^2	$G \times 10^{11}$ dyne/cm^2	σ	$Y \times 10^{11}$ dyne/cm^2	θ_D (K)
HB	H	0.9803	0.5660	0.1285	0.0771	0.2499	0.1928	58.42
	T	2.2841	1.3188	0.6977	0.4186	0.2499	1.0465	136.13
	IU	1.8280	1.0554	0.4469	0.2681	0.2499	0.6703	108.95
	F	1.6374	0.9454	0.3585	0.2151	0.2499	0.5378	97.58
	S	3.5473	2.0480	1.6826	1.0096	0.2500	2.5240	211.41
TG	H	1.5557	0.9006	0.3223	0.1952	0.2480	0.4873	92.94
	T	2.2458	1.3027	0.6693	0.4085	0.2464	1.0183	134.42
	IU	2.7705	1.6222	1.0030	0.6334	0.2392	1.5698	167.24
	F	2.6838	1.5683	0.9444	0.5920	0.2407	1.4690	161.71
	S	4.0634	2.4601	2.0320	1.4567	0.2107	3.5273	252.82
BS	H	4.9287	2.1162	4.4098	1.0779	0.3870	2.9901	222.34
	T	4.6220	1.4394	4.4771	0.4987	0.4463	1.4425	152.44
	IU	4.8145	1.7095	4.6413	0.7034	0.4279	2.0088	180.62
	F	4.7603	1.7137	4.5120	0.7069	0.4256	2.0154	181.00
	S	4.5767	1.4822	4.3367	0.5288	0.4414	1.5244	156.87

Table 4

Thermodynamic and Elastic Properties of $Ca_{60}Al_{40}$ Metallic Glass

App.	SCR	$\upsilon_L \times 10^5$ cm/sec	$\upsilon_T \times 10^5$ cm/s	$B_T \times 10^{11}$ dyne/cm^2	$G \times 10^{11}$ dyne/cm^2	σ	$Y \times 10^{11}$ dyne/cm^2	θ_D (K)
HB	H	2.1500	1.2413	0.4587	0.2752	0.2500	0.6880	128.78
	T	2.7311	1.5768	0.7401	0.4441	0.2500	1.1102	163.59
	IU	2.5999	1.5010	0.6707	0.4024	0.2500	1.0060	155.73
	F	2.6773	1.5458	0.7113	0.4268	0.2499	1.0669	160.37
	S	3.1795	1.8357	1.0031	0.6019	0.2499	1.5047	190.45
TG	H	3.5391	2.0550	1.2314	0.7543	0.2457	1.8792	213.10
	T	5.0526	2.9431	2.4969	1.5470	0.2432	3.8466	305.10
	IU	4.9460	2.9058	2.3585	1.5081	0.2364	3.7294	301.00
	F	5.0580	2.9755	2.4610	1.5813	0.2354	3.9071	308.18
	S	5.1593	3.0583	2.5269	1.6705	0.2291	4.1066	316.53
BS	H	7.1465	3.2489	6.6082	1.8852	0.3697	5.1645	342.27
	T	5.5428	1.3798	5.0339	0.3400	0.4670	0.9976	147.22
	IU	5.7036	1.7848	5.0517	0.5689	0.4457	1.6451	189.96
	F	5.7241	1.8886	5.0028	0.6371	0.4389	1.8334	200.84
	S	5.5616	1.1059	5.2333	0.2185	0.4794	0.6464	118.15

CONCLUSIONS

Three Ca-based metallic glasses are having important engineering application in the fields of materials science and technology. Therefore, it can be conclude that, as phonon dynamics and elastic properties of all these glasses have not been investigated theoretically previously. But the present study is very useful to form a set of theoretical data of particular glass and the present computations are also confirms the applicability of model potential in the aforesaid properties. Also, the PDC generated from three approaches reproduce all the broad characteristics of dispersion curves. But, the BS approach is found more qualitative than the others. The well known model potential with advanced IU, F and S-local field correction functions generates consistent results regarding the phonon dynamics of the metallic glasses. Such study on phonon dynamics of other binary liquid alloys and metallic glasses is in progress.

REFERENCES

1. P. N. Gajjar, A. M. Vora, A. R. Jani, *Proceedings of the 9th Asia Pacific Physics Conference Hanoi*, Vietnam (October 25–31, 2004) (2006) 429.
2. Aditya M. Vora, Chinese Physics Letters **23** 1872 (2006) 1872.
3. Aditya M. Vora, J. Non-Cryst. Sol. **352** 3217 (2006).
4. B. Y. Thakore, P. N. Gajjar, A. R. Jani, Bull. Mater. Sci. **23** 5 (2000).
5. J.–B. Suck, H. Rudin, H.–J. Güntherodt, H. Beck, J. Phys. C: Solid State Phys. **13** L1045 (1980); J. Phys. F: Met. Phys. **11** 1375 (1981); J. Phys. C: Solid State Phys. **14** 2305 (1981); Phys. Rev. Lett. **50** 49 (1983).
6. J. Hafner, Phys. Rev. **B27** 678 (1983).
7. J. Hafner, S. S. Jaswal, J. Phys. F: Met. Phys. **18** L1 (1988).
8. N. S. Saxena, Meeta Rani, Arun Pratap, Prabhu Ram, M. P. Saksena, Phys. Rev **B32** 8093 (1988).
9. N. S. Saxena, Arun Pratap, Deepika Bhandari, M. P. Saksena, Mater. Sci. Engg. **A134** 927 (1991).
10. P. C. Agarwal, K. A. Aziz, C. M. Kachhava, Acta Phys. Hung. **72** 183 (1992); Phys. Stat. Sol. (b) **178** 303 (1993).
11. P. C. Agarwal, C. M. Kachhava, Phys. Stat. Sol. (b) **179** 365 (1993); Ind. J. Pure & Appl. Phys. **31** 528 (1993).
12. M. Tegze, J. Hafner, J. Phys. Cond. Matt. **7** 8293 (1989); J. Non-Cryst. Sol. **117–118** 195 (1990).
13. J. Hafner, S. S. Jaswal, Phys. Rev. **B38** 7320 (1988).
14. J. Hubbard, J. L. Beeby, J. Phys. C: Solid State Phys. **2** 556 (1969).
15. S. Takeno, M. Goda, Prog. Thero. Phys. **45** 331 (1971); Prog. Thero. Phys. **47** 790 (1972).
16. A. B. Bhatia, R. N. Singh, Phys. Rev **B31** 4751 (1985).
17. M. M. Shukla, J. R. Campanha, Acta Phys. Pol. **A94** 655 (1998).
18. N. W. Ashcroft Phys. Lett. **23** 48 (1966).
19. W. A. Harrison, Pseudopotentials in the Theory of Metals, (W. A. Benjamin, Inc., New York, 1966).
20. R. Taylor, J. Phys. F: Met. Phys. **8** 1699 (1978).
21. S. Ichimaru, K. Utsumi, Phys. Rev. **B24** 3220 (1981).
22. B. Farid, V. Heine, G. E. Engel, I. J. Robertson, Phys. Rev. **B48** 11602 (1993).
23. A. Sarkar, D. S. Sen, S. Haldar, D. Roy, Mod. Phys. Lett. **B12** 639 (1998).